arXiv:2104.00921v2 [cs.CV] 10 Sep 2021

AAformer: Auto-Aligned Transformer for Person Re-Identification

Kuan Zhu[1] **Haiyun Guo**[1] **Shiliang Zhang**[3] **Yaowei Wang**[2] **Gaopan Huang**[4]
Honglin Qiao[4] **Jing Liu**[1] **Jinqiao Wang**[1] **Ming Tang**[1]

[1]Institute of Automation, Chinese Academy of Sciences
[2]Peng Cheng Laboratory, [3]Peking University, [4]Alibaba Group

Abstract

In person re-identification, extracting part-level features from person images has been verified to be crucial. Most of existing CNN-based methods only locate the human parts coarsely, or rely on pre-trained human parsing models and fail in locating the identifiable non-human parts (e.g., knapsack). In this paper, we introduce an alignment scheme in Transformer architecture for the first time and propose the Auto-Aligned Transformer (AAformer) to automatically locate both the human parts and non-human ones at patch-level. We introduce the "part tokens", which are learnable vectors, to extract part features in Transformer. A part token only interacts with a local subset of patches in self-attention and learns to be the part representation. To adaptively group the image patches into different subsets, we design the Auto-Alignment. Auto-Alignment employs a fast variant of Optimal Transport algorithm to online cluster the patch embeddings into several groups with the part tokens as their prototypes. We harmoniously integrate the part alignment into the self-attention and the output part tokens can be directly used for retrieval. Extensive experiments validate the effectiveness of part tokens and the superiority of AAformer over various state-of-the-art methods.

1 Introduction

Person re-identification (re-ID) aims to associate the specific person across cameras. Due to the inevitable problem of body part misalignment, which is caused by the inaccurate person detection, human pose variations, and the changing of camera viewpoints, lots of existing convolution neural network based methods extract part-level features to align the human parts and obtain fine-grained information. The stripe-based methods (Sun et al. 2018; Wang et al. 2018b; Zhang et al. 2018) design stripe-based image partition to locate human parts. Some methods adopt pre-trained human parsing models (Kalayeh et al. 2018; Alp Güler, Neverova, and Kokkinos 2018) to locate human parts of fine granularity. These methods either cannot well align the human parts or fail in locating the identifiable non-human parts like knapsack (Zhu et al. 2020; Kalayeh et al. 2018).

Recently, the self-attention based architecture, Transformer (Vaswani et al. 2017), has shown its scalability and effectiveness in many computer vision tasks. Dosovitskiy et al. (2020) first employs Transformer architecture to conduct image recognition. They divide the input image into fixed-size patches, linearly embed each of them and fed them to a Transformer encoder (Vaswani et al. 2017) to obtain the image representation. He et al. (2021) propose TransReID to apply the Transformer model (Dosovitskiy et al. 2020) to object re-identification. They design patch shuffle operations and introduce side information like camera/view IDs to learn robust features, validating the superiority of Transformer in re-ID task. As they do not take the misalignment issue into consideration, the part alignment scheme is still blank in Transformer architecture.

In this paper, we propose a specific alignment scheme for

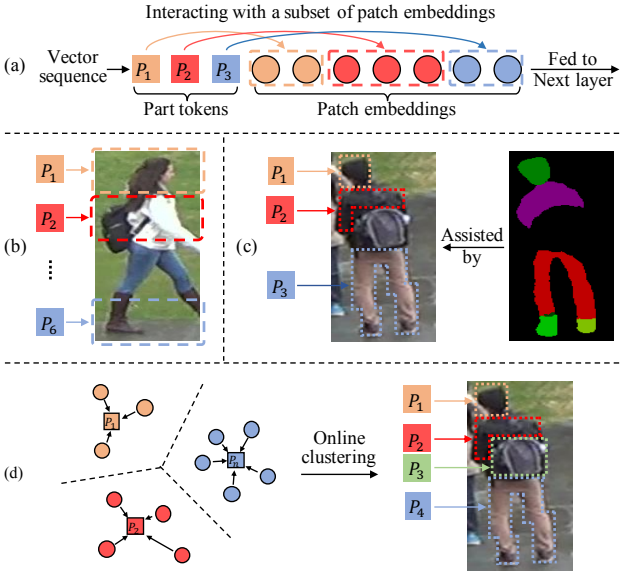


Figure 1: (a) The illustration of the added part tokens. A part token only interacts with a subset of patch embeddings thus can learn to represent the subset. (b) Part tokens with PCB's partitioning (Sun et al. 2018). (c) Part tokens with SPReID's partitioning (Kalayeh et al. 2018). (d) A toy example of the proposed Auto-Alignment. The image patches of the same part, which can be human part or non-human one, are adaptively grouped to the identical part token.

Transformer and also alleviate the existing alignment problems at the same time. We harmoniously integrate the part alignment into the self-attention of Transformer and propose Auto-Aligned Transformer (AAformer) to adaptively locate both the human parts and non-human ones at patch-level.

First, we propose the "part tokens", which are learnable vectors, for Transformer to learn the representations of local parts. Several part tokens are concatenated to the sequence of patch embeddings and subsequently fed to the Transformer encoder. In self-attention, a part token only attends to a local subset of patch embeddings and learns to represent the subset, which is shown in the first row of Figure 1. The part token with pre-defined fixed patch assignment (Sun et al. 2018; Kalayeh et al. 2018) is illustrated in the second row of Figure 1.

By means of the part token, we propose the Auto-Aligned Transformer (AAformer) to adaptively group the image patches into different subsets. We employ a fast variant of Optimal Transport algorithm (Cuturi 2013) to online cluster the patch embeddings into several groups with the part tokens as their prototypes (e.g., leg prototype, knapsack prototype). The patch embeddings of the same semantic part are gathered to the identical part token and the part token only interacts with these patch embeddings. Given an input image, the output part tokens of AAformer learn to be different part prototypes of patch subsets of the input image, and can be directly used as part features for re-ID. A toy example of this Auto-Alignment is shown in the last row of Figure 1. In each layer of AAformer, we sequentially conduct the Auto-Alignment to align the body parts and the Self-Attention to learn the part representations in the feedforward propagation. Rather than pre-defining the patch assignment for part alignment (Sun et al. 2018; Wang et al. 2018b; Kalayeh et al. 2018), AAformer simultaneously learns both part alignment and part representations online, thus can locate both human parts and non-human ones adaptively.

The contributions of this work are summarized as follows:

1) We introduce the "part tokens" for Transformer to learn part features and harmoniously integrate the part alignment into the self-attention. A part token only interacts with a subset of patch embeddings, thus can learn to be the local representation.

2) We further propose an Auto-Aligned Transformer (AAformer) to adaptively locate both the human parts and non-human ones online. Instead of using a pre-defined fixed patch assignment, AAformer simultaneously learns both part alignment and part representations.

3) Extensive experiments validate the effectiveness of part token and the superiority of AAformer over various state-of-the-art methods on four widely used benchmarks, i.e., Market-1501 (Zheng et al. 2015), DukeMTMC-reID (Zheng, Zheng, and Yang 2017), CUHK03 (Li et al. 2014; Zhong et al. 2017a) and MSMT17 (Wei et al. 2018).

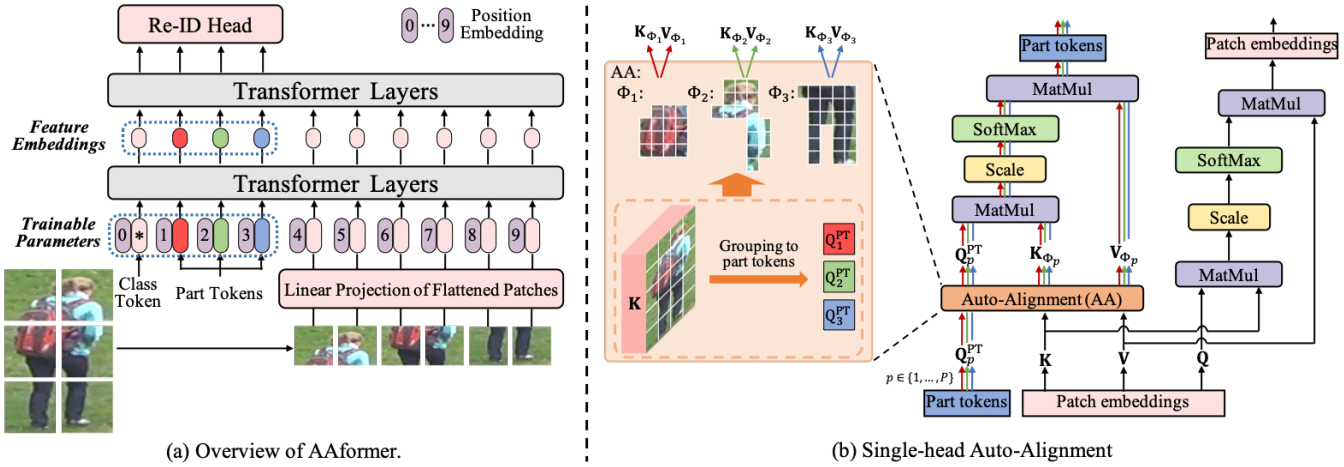
2 Related Work

2.1 Aligned Person Re-identification

The part misalignment issue is one of the most challenging problems for person re-ID. To remedy this, many efforts have been made to develop the aligned person re-ID. Some researchers develop stripe-based methods to extract part features (Sun et al. 2018; Wang et al. 2018b; Zhang et al. 2018). Sun et al. (2018) first directly partition the person images into fixed horizontal stripes and extract stripe-based part features. Wang et al. (2018b) enhance the robustness by dividing images into stripes of different granularities and design overlap between stripes. However, the stripe-based partition is too coarse to well align the human parts. Some other works employ extra semantics to locate human parts (Guo et al. 2019; Liu et al. 2018; Miao et al. 2019; Tay, Roy, and Yap 2019; Zheng et al. 2019a). Kalayeh et al. (2018) propose to employ a pre-trained human semantic parsing model to provide the mask of body parts for alignment. Zhang et al. (2019) adopt DensePose (Alp Güler, Neverova, and Kokkinos 2018) to obtain dense semantics of 24 regions for a person. However, the identifiable personal belongings like knapsack and reticule, which are crucial for person re-ID, cannot be recognized by the pre-trained models and ignored as background. Zhu et al. (2020) also propose to locate both human parts and non-human ones automatically by iterative clustering, but their off-line part partition is a little bit time-costing and prevents their method from end-to-end training. Besides, they use part pooling to generate part features, and this way is not suitable for Transformer as pooling is usually not applied in Transformer (Dosovitskiy et al. 2020; Devlin et al. 2019).

2.2 Visual Transformer

Transformer is proposed by (Vaswani et al. 2017) for machine translation and has since become the state-of-the-art architecture in many NLP tasks. Recently, the Transformer is showing its superiority over conventional methods in many vision tasks like object detection (Carion et al. 2020), generative adversarial network (Jiang, Chang, and Wang 2021), action recognition (Li et al. 2021a). Dosovitskiy et al. (2020) propose the Vision Transformer (ViT) to apply a pure Transformer to image recognition. They first divide the input image into image patches and then map them to a sequence of vectors with a linear projection. An extra learnable "class token (CLS)" is added to the sequence and the vector sequence is fed to a typical Transformer encoder. He et al. (2021) propose TransReID to apply ViT to object re-identification. They design patch shuffle operations and introduce side information like camera/view IDs to learn robust features, validating the superiority of Transformer on re-ID task. Li et al. (2021b) and Zhang et al. (2021) both integrate Transformer architecture into CNNs. Li et al. (2021b) propose to use Transformer to generate the attention masks for CNN and Zhang et al. (2021) use Transformer to aggregate hierarchical features from CNN backbones. However, as they do not design explicit alignment scheme to Transformer, how to extract discriminative part features from person images remains blank in Transformer architecture. In this paper, we aim to propose an adaptive alignment scheme for Transformer to solve the problems in existing alignment scheme of CNNs.



(a) Overview of AAformer. (b) Single-head Auto-Alignment

Figure 2: (a) The overview of AAformer. We divide the input image into fixed-size patches, linearly embed each of them and add the position embeddings. We add the extra learnable vectors of "class token (CLS)" and "part tokens" to learn the global and part representations of person images. The part tokens fed to the first Transformer layer are parameters of AAformer which learn the part prototypes of the datasets. The part tokens output by Transformer layers are learned feature embeddings to represent human parts for input images. (b) Single-head Auto-Alignment. The self-attention for part tokens is replaced by Auto-Alignment. $\mathbf{Q}^{\mathrm{PT}}$: *query* vectors of part tokens. Φ_p: the patches assigned to the pth part token. $\mathbf{Q}, \mathbf{K}, \mathbf{V}$: *query*, *key*, *value* vectors of patch embeddings.

3 Methodology

We begin by briefly revisiting the general Transformer architecture in Sect. 3.1. Then we present the proposed part token and the Auto-Aligned Transformer (AAformer) in Sect. 3.2.

3.1 The Main Architecture

We follow Vision Transformer (ViT) (Dosovitskiy et al. 2020) to construct the main architecture. Given an input image $\mathbf{x} \in \mathbb{R}^{H \times W \times C}$ with resolution (H, W) and channel C, we reshape it into a sequence of flattened 2D patches $\mathbf{x} \in \mathbb{R}^{N \times (I^2 \cdot C)}$ to fit the Transformer architecture, where (I, I) is the resolution of each image patch and $N = (H \cdot W)/I^2$ is the length of image patch sequence. We map the patches to vectors of D dimensions with a trainable linear projection and refer to the output of this projection as the patch embeddings. A standard embedding of "class token (CLS)" is added to extract the global representation. Lastly, the outcome vector sequence $\mathbf{Z} \in \mathbb{R}^{L \times D}$ is fed to the Transformer encoder, where $L = 1+N$. We also add the standard learnable 1D position embeddings to the vector sequence in element-wise to retain positional information.

The standard Transformer layer (Vaswani et al. 2017) consists of Multi-head Self-Attention (MSA) and Multi-Layer Perception (MLP) blocks. The self-attention mechanism is based on a trainable associative memory with key and $value$ vector pairs. For every $query$ vector in a sequence of query vectors ($\mathbf{Q} \in \mathbb{R}^{L \times D}$), we calculate its inner products with a set of key vectors ($\mathbf{K} \in \mathbb{R}^{L \times D}$). These inner products are then scaled and normalized with a softmax function to obtain L weights. The output of the self-attention for this $query$ is the weighted sum of a set of L $value$ vectors ($\mathbf{V} \in \mathbb{R}^{L \times D}$). For all the $queries$ in the sequence, the output matrix of self-attention can be obtained by:

$$Attention(\mathbf{Q}, \mathbf{K}, \mathbf{V}) = Softmax(\frac{\mathbf{Q}\mathbf{K}^T}{\sqrt{D}})\mathbf{V}, \quad (1)$$

where the $Softmax$ function is applied over each row of the input matrix and the $\sqrt{D}$ term provides appropriate normalization. $Query$, key and $value$ matrices are all computed from the vector sequence $\mathbf{Z}$ using different linear transformations: $\mathbf{Q} = \mathbf{Z}\mathbf{W}_Q$, $\mathbf{K} = \mathbf{Z}\mathbf{W}_K$, $\mathbf{V} = \mathbf{Z}\mathbf{W}_V$. Finally, the Multi-head Self-Attention layer (MSA) is defined by considering h attention "heads", i.e., h self-attention functions are applied to the input in parallel. Each head provides a sequence of size $L \times d$, where $d = D/h$ typically. The outputs of the h self-attention are rearranged into a $L \times D$ sequence to feed the next Transformer layer.

The MSA is followed by a MLP block to build a full Transformer layer as in (Vaswani et al. 2017). This MLP contains two linear layers separated by a GELU non-linearity (Hendrycks and Gimpel 2016). The first linear layer expands the dimension from D to $4D$ and the second reduces the dimension back to D. Both MSA and MLP are operating as residual connections and with a layer normalization (LN) (Ba, Kiros, and Hinton 2016) before them. **We change the MSA layer to Multi-head Auto-Alignment (MAA) layer to build our AAformer.** The overview of AAformer is shown in the left part of Figure 2.

3.2 Auto-Aligned Transformer

Part tokens for Transformer. We propose the "part tokens" for Transformer to extract the part features and integrate the part alignment into self-attention. We concatenate P "part tokens", which are learnable vectors, to the sequence

$\mathbf{Z}$, thus now the length L of $\mathbf{Z}$ is $1+P+N$. A part token only interacts with a subset of patch embeddings, rather than all of them, thus can learn to be the part representation of the subset. Specifically, we denote $\mathbf{Q}^{\mathrm{PT}} = [\mathbf{Q}_1^{\mathrm{PT}}, ..., \mathbf{Q}_P^{\mathrm{PT}}]$ as the $query$ vectors of part tokens and denote Φ_p as the subset of patch embeddings assigned to the pth part token. For the $query$ vector of the pth part token, denoted as $\mathbf{Q}_p^{\mathrm{PT}}$, we only calculate its inner products with the key vectors belonging to Φ_p and then scale and normalize these inner products with softmax function to obtain $len(\Phi_p)$ weights. The output of the part alignment for $\mathbf{Q}_p^{\mathrm{PT}}$ is the weighted sum of *value* vectors belonging to Φ_p, which is formulated as:

$$Alignment(\mathbf{Q}_p^{\mathrm{PT}}, \mathbf{K}, \mathbf{V}) = Softmax(\frac{\mathbf{Q}_p^{\mathrm{PT}}\mathbf{K}_{\Phi_p}^T}{\sqrt{D}})\mathbf{V}_{\Phi_p}, \tag{2}$$

where $\mathbf{K}_{\Phi_p}$ and $\mathbf{V}_{\Phi_p}$ are the key and $value$ vectors belonging to Φ_p, respectively. After the part alignment, the output vector of part token p becomes the part representation of subset Φ_p. The CLS token and patch embeddings are processed by the original self-attention (Eq. 1).

Now, to extract discriminative part features, the core problem is how to accurately and adaptively assign image patches to $\Phi_p, p \in \{1, ..., P\}$.

Multi-head Auto-Alignment. The Auto-Alignment aims at automatically grouping the image patches into different Φ_p ($p \in \{1, ..., P\}$), in which both human parts and non-human ones are included. The Φ_p for different part tokens should be mutually exclusive. Our idea is adaptively clustering the patch embeddings into P groups with the part tokens as their prototypes. This makes the patch assignment problem the same as the Optimal Transport problem (Cuturi 2013). In detail, the $query$ vectors of part tokens, $\mathbf{Q}^{\mathrm{PT}} \in \mathbb{R}^{P\times D}$, are regarded as the part prototypes, and we are interested in mapping the key vectors of image patches $\mathbf{K} \in \mathbb{R}^{N\times D}$ to the $\mathbf{Q}^{\mathrm{PT}}$ to obtain the patch assignment (CLS token does not participate in the clustering and is omitted for simplicity). We denote this mapping by $\mathbf{Y} \in \mathbb{R}^{P\times N}$, and the value in position (p, n) denotes the probability of the nth image patch belonging to the pth part token. To maximize the similarity between $\mathbf{K}$ and $\mathbf{Q}^{\mathrm{PT}}$, $\mathbf{Y}$ is optimized by:

$$\max_{\mathbf{Y}\in\mathcal{Y}} \mathrm{Tr}\left(\mathbf{Y}^\top \mathbf{Q}^{\mathrm{PT}} \mathbf{K}^\top\right) + \varepsilon H(\mathbf{Y}), \tag{3}$$

where $\mathrm{Tr}\left(\mathbf{Y}^\top \mathbf{Q}^{\mathrm{PT}} \mathbf{K}^\top\right)$ measures the similarity between $\mathbf{K}$ and $\mathbf{Q}^{\mathrm{PT}}$, $H(\mathbf{Y}) = -\sum_{ij} \mathbf{Y}_{ij} \log \mathbf{Y}_{ij}$ is the entropy function, and ε is the parameter that controls the smoothness of the mapping and is set to be 0.05 in our experiments.

To further prevent the trivial solution where all the patches are assigned to the same part token, we enforce an equal partition by constraining the matrix $\mathbf{Y}$ to belong to the transportation polytope (Asano, Rupprecht, and Vedaldi 2019; Caron et al. 2020). We adapt this constraint to patch assignment by restricting the transportation polytope to the image patches of an image:

$$\mathcal{Y} = \left\{ \mathbf{Y} \in \mathbb{R}_+^{P\times N} \mid \mathbf{Y}\mathbb{1}_N = \frac{1}{P}\mathbb{1}_P, \mathbf{Y}^\top \mathbb{1}_P = \frac{1}{N}\mathbb{1}_N \right\}, \tag{4}$$

where $\mathbb{1}_P$ denotes the vector of ones in dimension P. These constraints enforce that on average each part token is selected at least N/P times in an image. The soft assignment $\mathbf{Y}^*$ are the solution to Prob. 3 over the set $\mathcal{Y}$ and takes the form of a normalized exponential matrix (Cuturi 2013):

$$\mathbf{Y}^* = \mathrm{Diag}(\mathbf{u}) \exp\left(\frac{\mathbf{Q}^{\mathrm{PT}}\mathbf{K}^\top}{\varepsilon}\right) \mathrm{Diag}(\mathbf{v}), \tag{5}$$

where $\mathbf{u}$ and $\mathbf{v}$ are renormalization vectors in $\mathbb{R}^P$ and $\mathbb{R}^N$ respectively. These renormalization vectors are computed using a small number of matrix multiplications by a fast variant of Sinkhorn-Knopp algorithm (Cuturi 2013). This algorithm can be efficiently run on GPU and we observe that only 3 iterations is sufficient to obtain good performance for patch assignment. In our experiments, grouping 576 patch embeddings of an image to 5 part tokens only takes 0.46ms. Once a continuous solution $\mathbf{Y}^*$ is found, the patch assignment can be obtained by using a rounding procedure. The patch embeddings mapped to $\mathbf{Q}_p^{\mathrm{PT}}$ are the patch subset Φ_p. We illustrate the Auto-Alignment process (single-head) in the right part of Figure 2. The Auto-Alignment are conducted in parallel in different attention heads, which enhances the robustness of patch assignment. We name this Multi-head Auto-Alignment (MAA) and the outputs of different attention heads are concatenated together. The output part tokens of AAformer are used to perform person re-ID.

In each layer of AAformer, we conduct the Auto-Alignment to align the body parts and the Self-Attention to learn the part representations in the feedforward propagation. Therefore, AAformer is an online method that simultaneously learns both part alignment and part representations.

Discussion on part token in AAformer. (1) The part tokens fed to the first Transformer layer are learnable parameters of AAformer as shown in Figure 2. After continually interacting with the patch embeddings of the same sematic part of different person identities during training, each part token learns to be a part prototype of dataset. This also guarantees the semantic consistency throughout the dataset. (2) After the input part tokens of the first Transformer layer interacting with the patch embeddings of an input image, the produced part tokens of all Transformer layers will be the part prototypes and feature embeddings of the patch subsets of the input image. On the other words, the produced part tokens of each Transformer layer are instance-adaptive. That is, they are the part representatives of the input images. Consequently, they can be employed directly as part features for the re-ID task.

3.3 Objective Function

In the training phase, the re-ID heads (Luo et al. 2019) are attached to the output CLS and part tokens of AAformer. Specifically, the output CLS $\mathbf{Z}_0$ represents the global feature of the input image, and the output part tokens $\mathbf{Z}_{1:P}$ are the part features. We employ the commonly used triplet loss (Hermans, Beyer, and Leibe 2017) and cross-entropy loss to train our model. The cross-entropy loss is calculated as:

$$L_{cls} = \frac{1}{P+1}\sum_{i=0}^{P} -\log \mathcal{P}(\mathbf{Z}_i), \tag{6}$$

where $\mathcal{P}(\mathbf{Z}_i)$ is the probability of token $\mathbf{Z}_i$ belonging to its ground truth identity. The classifiers of different tokens are not shared. Label smoothing (Szegedy et al. 2016) is adopted to improve the performance.

The part tokens $\mathbf{Z}_{1:P}$ are concatenated together to calculate the part triplet loss. Together with the global triplet loss calculated with CLS, there are two terms in the triplet loss:

$$L_{tri} = \frac{1}{2}\left([d_p^g - d_n^g + \alpha]_+ + [d_p^p - d_n^p + \alpha]_+\right), \quad (7)$$

where d_p^g and d_n^g are feature distances of global representation (CLS) from positive pair and negative pair, respectively. d_p^p and d_n^p are feature distances of concatenated part tokens from positive pair and negative pair, respectively. α is the margin of triplet loss and is set to 0.3 in our experiments. $[\cdot]_+$ equals to $max(\cdot, 0)$. Therefore, the overall objective function for our model is:

$$L = L_{cls} + L_{tri}. \quad (8)$$

In the testing phase, CLS and part tokens are concatenated together to represent a person image.

4 Experiments

4.1 Implementation Details and Datasets

The Transformer architecture. We use the smallest Vision Transformer model proposed in (Dosovitskiy et al. 2020), which is named as ViT-Base, as the main architecture of AAformer. It contains 12 Transformer layers with the hidden size of 768 dimensions ($D=768$). The MLP size is 4 times the hidden size and the head number is 12 for multi-head operations.

Data preprocessing. The input images are resized to 384×256 and the patch size is 16×16. We adopt the commonly used random cropping (Wang et al. 2018d), horizontal flipping and random erasing (Wang et al. 2018a,d; Zhong et al. 2017b) (with a probability of 0.5) for data augmentation.

Training. The Transformer backbone is initialized with the pre-trained parameters on ImageNet (Deng et al. 2009). We observe that, on re-ID datasets, it only needs 24 epochs for AAformer to converge, which is $1/5$ of that for CNN models. We warm up the model for 2 epochs with a linearly growing learning rate from 3.5×10^{-5} to 3.5×10^{-4}. Then, the learning rate is decreased by a factor of 0.1 at the 8th and 14th epoch. The batch size is set to 128 and Adam (Kingma and Ba 2014) method is adopted to optimize the model. The results are the average of three runs of the codes. All our methods are implemented on PyTorch and we use 4 NVIDIA Tesla V100 GPUs for training.

Datasets and Evaluation Metrics. We conduct experiments on four widely used holistic person re-ID benchmarks, i.e., Market-1501 (Zheng et al. 2015), DukeMTMC-reID (Zheng, Zheng, and Yang 2017), CUHK03 (New Protocol) (Li et al. 2014; Zhong et al. 2017a), and the large-scale MSMT17 (Wei et al. 2018). We adopt the standard training/test ID split, which is detailed in Table 1. We also evaluate the performance of AAformer on the occluded re-ID benchmark, Occluded-DukeMTMC (Miao et al. 2019), which is by far the largest and the only occluded person re-ID dataset that contains training set. Following common practices, we use the cumulative matching characteristics (CMC) at Rank-1 (R-1) and the mean average precision (mAP) to evaluate the performance.

Table 1: Re-ID datasets and details.

Dataset	#ID	#Train	#Test	#Images
Market-1501	1501	751	750	32668
DukeMTMC-reID	1402	702	702	36411
CUHK03	1467	767	700	14097
MSMT17	4101	1041	3060	126441

4.2 Comparison with State-of-the-art Methods

We compare our method with the state-of-the-art methods on four widely used holistic benchmarks and one occluded benchmark in Table 2 and Table 3. We also show the results of ViT-baseline (Dosovitskiy et al. 2020) in the tables.

DukeMTMC-reID. AAformer obtains the best results and outperforms others by at least 1.3% on both Rank-1 and mAP. The compared methods are categorized into three groups, i.e., stripe-based methods, extra semantics-based methods, and others. The others include the general attention methods based on CNN (Hou et al. 2019; Zheng et al. 2019b), the work that combines self-attention with CNN (Wang et al. 2018c; Li et al. 2021b) and the method based on generative adversarial network (Zheng et al. 2019c). AAformer surpasses all the above methods by considerable margins, which validates the superiority of locating both human parts and non-human ones.

Market1501. AAformer achieves state-of-the-art performance. Specifically, AAformer obtains the second-best result and is only 0.3% behind the first (Wang et al. 2018b; Li et al. 2021b). As the performance on this dataset is nearly saturated, the results of these sate-of-the-art methods are very close.

CUHK03. AAformer obtains the best performance on both labeled and detected sets. More specifically, AAformer outperforms the second-best algorithm, i.e., BAT-net, by $1.3\%/1.7\%$ and $1.4\%/1.6\%$ on labeled and detected sets with regards to Rank-1 and mAP accuracy. AAformer also significantly improves the ViT-baseline by $3.2 \sim 4.5\%$, which validates the effectiveness of our Multi-head Auto-Alignment.

MSMT17. On the largest dataset, we follow (He et al. 2021) to conduct an overlap of four pixels between adjacent image patches. On the metric of Rank-1, AAformer outperforms the second-best (He et al. 2021) by a large margin, i.e., 1.1%. On the metric of mAP, AAformer obtains the comparable accuracy with (He et al. 2021).

Occluded-DukeMTMC. AAformer sets the new state-of-the-art performance and outperforms others by a large margin, at least $2.5\%/4.6\%$ in Rank-1/mAP. Owing to the Auto-Alignment, the part tokens can adaptively focus on the visible areas in the occluded images and extract discriminative features from these visible areas. We also visualize the attention maps of part tokens in the Sect. 4.3 to validate this.

Methods	DukeMTMC -reID		Market1501		CUHK03				MSMT17	
					Labeled		Detected			
	R-1	mAP	R-1	mAP	R-1	mAP	R-1	mAP	R-1	mAP
AlignedReID (Zhang et al. 2018)	-	-	91.8	79.3	-	-	-	-	-	-
PCB+RPP (Sun et al. 2018)	83.3	69.2	93.8	81.6	-	-	63.7	57.5	68.2	40.4
MGN (Wang et al. 2018b)	88.7	78.4	**95.7**	86.9	68.0	67.4	66.8	66.0	-	-
SPReID (Kalayeh et al. 2018)	84.4	71.0	92.5	81.3	-	-	-	-	-	-
PABR (Suh et al. 2018a)	84.4	69.3	91.7	79.6	-	-	-	-	-	-
AANet (Tay, Roy, and Yap 2019)	87.7	74.3	93.9	83.4	-	-	-	-	-	-
P^2-Net (Guo et al. 2019)	86.5	73.1	95.2	85.6	78.3	73.6	74.9	68.9	-	-
PGFA (Miao et al. 2019)	82.6	65.5	91.2	76.8	-	-	-	-	-	-
GASM (He and Liu 2020)	88.3	74.4	95.3	84.7	-	-	-	-	79.5	52.5
IANet (Hou et al. 2019)	87.1	73.4	94.4	83.1	-	-	-	-	75.5	46.8
CASN+PCB (Zheng et al. 2019b)	87.7	73.7	94.4	82.8	73.7	68.0	71.5	64.4	-	-
BAT-net (Fang et al. 2019)	87.7	77.3	95.1	84.7	78.6	76.1	76.2	73.2	79.5	56.8
Non-Local (Wang et al. 2018c)	88.6	78.7	94.9	86.8	66.4	65.0	65.3	63.1	76.2	53.3
JDGL (Zheng et al. 2019c)	86.6	74.8	94.8	86.0	-	-	-	-	77.2	52.3
OSNet (Zhou et al. 2019)	88.6	73.5	94.8	84.9	-	-	72.3	67.8	78.7	52.9
PAT (Li et al. 2021b)	88.8	78.2	95.4	**88.0**	-	-	-	-	-	-
TransReID* (He et al. 2021)	-	-	-	-	-	-	-	-	82.5	**63.6**
ViT-baseline	88.2	78.3	94.2	86.1	75.4	74.6	74.0	71.3	79.4	58.5
AAformer (ours)	**90.1**	**80.0**	95.4	87.7	**79.9**	**77.8**	**77.6**	**74.8**	**83.6**	63.2

Table 2: Comparison with state-of-the-art CNN-based methods for the holistic person re-ID problem. Methods in the 1st group are the stripe-based methods. Methods in the 2nd group are extra semantics-based methods. Methods in the 3rd group include the general attention methods of CNN (Hou et al. 2019; Zheng et al. 2019b), the work that combines self-attention with CNN (Wang et al. 2018c; Li et al. 2021b) and the method based on pure Transformer (He et al. 2021) ($*$ means no side information).

Methods	R-1	R-5	mAP
PCB (Sun et al. 2018)	42.6	57.1	33.7
Part Bilinear (Suh et al. 2018b)	36.9	-	-
FD-GAN (Ge et al. 2018)	40.8	-	-
DSR (He et al. 2018a)	40.8	58.2	30.4
SFR (He et al. 2018b)	42.3	60.3	32.0
PGFA (Miao et al. 2019)	51.4	68.6	37.3
HOReID (Wang et al. 2020)	55.1	-	43.8
PAT (Li et al. 2021b)	64.5	-	53.6
ViT-baseline	60.7	77.6	52.3
AAformer (ours)	**67.0**	**81.5**	**58.2**

Table 3: Comparison with state-of-the-art methods for the occluded re-ID problem on Occluded-DukeMTMC.

4.3 Ablation Studies

The effectiveness of the "part tokens". We first conduct experiments to validate the effectiveness of part tokens. We begin by naively adopting the alignment paradigm of CNNs, i.e., part masks with part pooling, to the baseline Transformer model (ViT-Base), and choose three typical methods, i.e., PCB (Sun et al. 2018), MGN (Wang et al. 2018b) and SPReID (Kalayeh et al. 2018). The first two methods are stripe-based methods and the third method adopts the extra semantics. As shown in Table 4, naively applying the alignment paradigm of CNNs even reduces the performance of the baseline model, which may be because pooling is not suitable for Transformer.

Next, we discard the pooling operation and add the proposed part tokens to ViT to extract part features. The typical image partitions of CNN-based methods are adopted for fair comparison, e.g., we assign each part token with patches within a stripe to simulate the image partition of PCB. As shown in Table 4, models with part tokens bring consistent improvement to the baseline, validating the effectiveness of part tokens in extracting part features for Transformer.

Besides, to prove the improvement is not brought by the increase of feature dimension, we conduct the experiment which directly adds more CLS tokens to ViT. The results in Table 4 validate naively increasing the feature dimension can not improve the performance as the information contained in these CLS tokens is repetitive and redundant.

The effectiveness of AAformer. Further, considering that the stripe-based patch assignments can not well align human parts and the extra semantics can not recognize the identifiable non-human parts like knapsack (Zhu et al. 2020; Guo et al. 2019), we propose AAformer to automatically locate both human parts and non-human ones at patch-level. As shown in the last row of Table 4, AAformer surpasses all the typical alignment methods reimplemented on part tokens by large margins, which validates the superiority of online adaptive patch assignment over the fixed patterns.

Optimal Transport *vs.* Nearest Neighbor. The most naive way to adaptively assign the patch embeddings is using the Nearest Neighbor algorithm, which assigns the patch embedding to the nearest part token. Unfortunately, in our

Methods	Scheme	DukeMTMC -reID		CUHK03(L)	
		R-1	mAP	R-1	mAP
ViT-baseline	None	88.2	78.3	75.4	74.6
+PCB	Pool	88.1	78.2	76.2	75.2
+MGN	Pool	88.6	78.3	76.4	74.8
+SPReID	Pool	86.9	76.5	74.9	73.0
+PCB	PT	89.1	78.9	78.3	76.5
+MGN	PT	89.3	79.1	78.5	76.6
+SPReID	PT	88.9	78.7	79.0	76.9
ViT-baseline	6*CLS	88.4	78.3	75.5	74.9
AAformer	PT	**90.1**	**80.0**	**79.9**	**77.8**

Table 4: The effectiveness of part tokens and AAformer. "Pool" means "Pooling" and "PT" means "Part tokens".

Settings	DukeMTMC-reID		CUHK03(L)	
	R-1	mAP	R-1	mAP
Nearest Neighbor	89.3	79.2	78.8	76.9
Optimal Transport	**90.1**	**80.0**	**79.9**	**77.8**

Table 5: The comparison of patch assignment with the Nearest Neighbor and the Optimal Transport algorithm.

experiments, we observe that most patch embeddings are grouped to the same part token when adopting the Nearest Neighbor algorithm as there is no constraint on the patch assignment. The results in Table 5 also demonstrate the superiority of Optimal Transport.

Different granularity for AAformer. Intuitively, the number of part tokens P determines the granularity of the body parts. Thanks to the flexibility of AAformer, one can set multiple sets of part tokens with different granularity for an AAformer model, which means partitioning the image with different granularity in parallel. For example, granularity $\{2, 3\}$ indicates there are totally 5 part tokens added. The first two part tokens divide the image patches into two groups and the last three part tokens divide them into three. The results of AAformer with different granularity are shown in Table 6. We observe that the setting of granularity $\{2, 3\}$ usually obtains the best accuracy, which is consistent with the setting of MGN. All the previous results of AAformer on different datasets are obtained with the default setting of granularity $\{2, 3\}$.

P	DukeMTMC-reID		CUHK03(L)	
	R-1	mAP	R-1	mAP
{4}	89.5	79.8	78.4	76.7
{5}	89.1	79.4	79.8	77.6
{6}	89.2	79.8	79.0	77.1
{2,3}	**90.1**	**80.0**	**79.9**	**77.8**
{3,4}	90.0	79.7	79.1	77.5
{2,3,4}	89.8	79.6	78.7	77.4

Table 6: Ablation studies on different granularity.

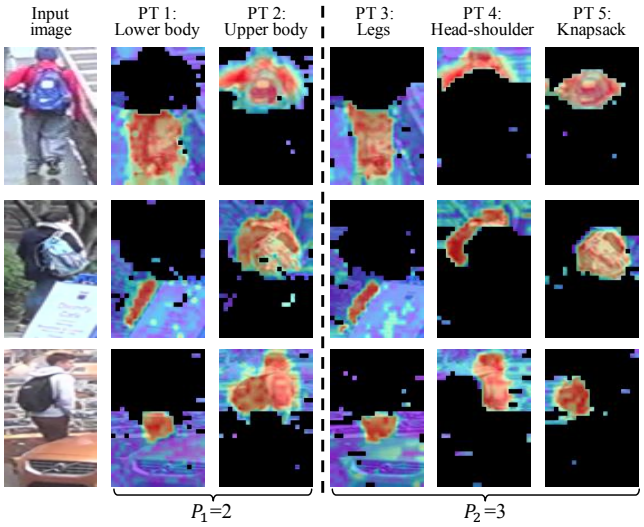


Figure 3: The attention map of part tokens (PT). The patches masked by black mean they are not assigned to this part token. The color blue to red indicates that the attention is getting higher and higher.

Visualization of AAformer. Lastly, we conduct the visualization experiments to show the focusing areas of part tokens. We visualize the attentnion map of part tokens in the first head of the third Transformer layer, which is shown in Figure 3. As we can observe, AAformer can focus on both human parts and non-human ones, which are both crucial for re-ID. This is also the main superiority of AAformer over existing methods. Owing to the self-attention mechanism, the part tokens have very low responses to the background patches, thus it is no need for AAformer to remove the background patches. The visualization also proves the semantics consistency of the located parts among images, which is analysed in the end of Sect. 3.2.

5 Conclusion

In this paper, we propose the "part tokens" for Transformer and harmoniously integrate the part alignment into the self-attention to learn part representations. We also propose the Auto-Aligned Transformer (AAformer) to adaptively locate both human parts and non-human ones. Extensive experiments validate the effectiveness of part tokens and the superiority of AAformer over lots of state-of-the-art methods.

References

Alp Güler, R.; Neverova, N.; and Kokkinos, I. 2018. Densepose: Dense human pose estimation in the wild. In *Proceedings of the IEEE Conference on Computer Vision and Pattern Recognition*, 7297–7306.

Asano, Y. M.; Rupprecht, C.; and Vedaldi, A. 2019. Self-labelling via simultaneous clustering and representation learning. *arXiv preprint arXiv:1911.05371*.

Ba, J. L.; Kiros, J. R.; and Hinton, G. E. 2016. Layer normalization. *arXiv preprint arXiv:1607.06450*.

Carion, N.; Massa, F.; Synnaeve, G.; Usunier, N.; Kirillov, A.; and Zagoruyko, S. 2020. End-to-end object detection with transformers. In *European Conference on Computer Vision*, 213–229. Springer.

Caron, M.; Misra, I.; Mairal, J.; Goyal, P.; Bojanowski, P.; and Joulin, A. 2020. Unsupervised learning of visual features by contrasting cluster assignments. *arXiv preprint arXiv:2006.09882*.

Cuturi, M. 2013. Sinkhorn distances: Lightspeed computation of optimal transport. *Advances in neural information processing systems*, 26: 2292–2300.

Deng, J.; Dong, W.; Socher, R.; Li, L.-J.; Li, K.; and Fei-Fei, L. 2009. Imagenet: A large-scale hierarchical image database. In *2009 IEEE conference on computer vision and pattern recognition*, 248–255. Ieee.

Devlin, J.; Chang, M.-W.; Lee, K.; and Toutanova, K. 2019. BERT: Pre-training of Deep Bidirectional Transformers for Language Understanding. In *NAACL-HLT (1)*.

Dosovitskiy, A.; Beyer, L.; Kolesnikov, A.; Weissenborn, D.; Zhai, X.; Unterthiner, T.; Dehghani, M.; Minderer, M.; Heigold, G.; Gelly, S.; et al. 2020. An image is worth 16x16 words: Transformers for image recognition at scale. *arXiv preprint arXiv:2010.11929*.

Fang, P.; Zhou, J.; Roy, S. K.; Petersson, L.; and Harandi, M. 2019. Bilinear attention networks for person retrieval. In *Proceedings of the IEEE/CVF International Conference on Computer Vision*, 8030–8039.

Ge, Y.; Li, Z.; Zhao, H.; Yin, G.; Yi, S.; Wang, X.; et al. 2018. Fd-gan: Pose-guided feature distilling gan for robust person re-identification. In *Advances in neural information processing systems*, 1222–1233.

Guo, J.; Yuan, Y.; Huang, L.; Zhang, C.; Yao, J.-G.; and Han, K. 2019. Beyond Human Parts: Dual Part-Aligned Representations for Person Re-Identification. In *The IEEE International Conference on Computer Vision (ICCV)*.

He, L.; Liang, J.; Li, H.; and Sun, Z. 2018a. Deep spatial feature reconstruction for partial person re-identification: Alignment-free approach. In *Proceedings of the IEEE Conference on Computer Vision and Pattern Recognition*, 7073–7082.

He, L.; and Liu, W. 2020. Guided Saliency Feature Learning for Person Re-identification in Crowded Scenes. In *European Conference on Computer Vision*.

He, L.; Sun, Z.; Zhu, Y.; and Wang, Y. 2018b. Recognizing partial biometric patterns. *arXiv preprint arXiv:1810.07399*.

He, S.; Luo, H.; Wang, P.; Wang, F.; Li, H.; and Jiang, W. 2021. Transreid: Transformer-based object re-identification. In *Proceedings of the IEEE International Conference on Computer Vision*.

Hendrycks, D.; and Gimpel, K. 2016. Gaussian error linear units (gelus). *arXiv preprint arXiv:1606.08415*.

Hermans, A.; Beyer, L.; and Leibe, B. 2017. In defense of the triplet loss for person re-identification. *arXiv preprint arXiv:1703.07737*.

Hou, R.; Ma, B.; Chang, H.; Gu, X.; Shan, S.; and Chen, X. 2019. Interaction-And-Aggregation Network for Person Re-Identification. In *The IEEE Conference on Computer Vision and Pattern Recognition (CVPR)*.

Jiang, Y.; Chang, S.; and Wang, Z. 2021. TransGAN: Two Transformers Can Make One Strong GAN. *arXiv preprint arXiv:2102.07074*.

Kalayeh, M. M.; Basaran, E.; Gökmen, M.; Kamasak, M. E.; and Shah, M. 2018. Human semantic parsing for person re-identification. In *Proceedings of the IEEE Conference on Computer Vision and Pattern Recognition*, 1062–1071.

Kingma, D. P.; and Ba, J. 2014. Adam: A method for stochastic optimization. *arXiv preprint arXiv:1412.6980*.

Li, W.; Zhao, R.; Xiao, T.; and Wang, X. 2014. Deepreid: Deep filter pairing neural network for person re-identification. In *Proceedings of the IEEE conference on computer vision and pattern recognition*, 152–159.

Li, X.; Hou, Y.; Wang, P.; Gao, Z.; Xu, M.; and Li, W. 2021a. Trear: Transformer-based RGB-D Egocentric Action Recognition. *arXiv preprint arXiv:2101.03904*.

Li, Y.; He, J.; Zhang, T.; Liu, X.; Zhang, Y.; and Wu, F. 2021b. Diverse Part Discovery: Occluded Person Re-Identification With Part-Aware Transformer. In *Proceedings of the IEEE/CVF Conference on Computer Vision and Pattern Recognition*, 2898–2907.

Liu, J.; Ni, B.; Yan, Y.; Zhou, P.; Cheng, S.; and Hu, J. 2018. Pose transferrable person re-identification. In *Proceedings of the IEEE Conference on Computer Vision and Pattern Recognition*, 4099–4108.

Luo, H.; Gu, Y.; Liao, X.; Lai, S.; and Jiang, W. 2019. Bag of tricks and a strong baseline for deep person re-identification. In *Proceedings of the IEEE Conference on Computer Vision and Pattern Recognition Workshops*, 0–0.

Miao, J.; Wu, Y.; Liu, P.; Ding, Y.; and Yang, Y. 2019. Pose-Guided Feature Alignment for Occluded Person Re-Identification. In *The IEEE International Conference on Computer Vision (ICCV)*.

Suh, Y.; Wang, J.; Tang, S.; Mei, T.; and Mu Lee, K. 2018a. Part-aligned bilinear representations for person re-identification. In *Proceedings of the European Conference on Computer Vision (ECCV)*, 402–419.

Suh, Y.; Wang, J.; Tang, S.; Mei, T.; and Mu Lee, K. 2018b. Part-aligned bilinear representations for person re-identification. In *Proceedings of the European Conference on Computer Vision (ECCV)*, 402–419.

Sun, Y.; Zheng, L.; Yang, Y.; Tian, Q.; and Wang, S. 2018. Beyond part models: Person retrieval with refined part pooling (and a strong convolutional baseline). In *Proceedings of the European Conference on Computer Vision (ECCV)*, 480–496.

Szegedy, C.; Vanhoucke, V.; Ioffe, S.; Shlens, J.; and Wojna, Z. 2016. Rethinking the inception architecture for computer vision. In *Proceedings of the IEEE conference on computer vision and pattern recognition*, 2818–2826.

Tay, C.-P.; Roy, S.; and Yap, K.-H. 2019. AANet: Attribute Attention Network for Person Re-Identifications. In *The*

IEEE Conference on Computer Vision and Pattern Recognition (CVPR).

Vaswani, A.; Shazeer, N.; Parmar, N.; Uszkoreit, J.; Jones, L.; Gomez, A. N.; Kaiser, Ł.; and Polosukhin, I. 2017. Attention is all you need. In *Proceedings of the 31st International Conference on Neural Information Processing Systems*, 6000–6010.

Wang, C.; Zhang, Q.; Huang, C.; Liu, W.; and Wang, X. 2018a. Mancs: A multi-task attentional network with curriculum sampling for person re-identification. In *Proceedings of the European Conference on Computer Vision (ECCV)*, 365–381.

Wang, G.; Yang, S.; Liu, H.; Wang, Z.; Yang, Y.; Wang, S.; Yu, G.; Zhou, E.; and Sun, J. 2020. High-order information matters: Learning relation and topology for occluded person re-identification. In *Proceedings of the IEEE/CVF Conference on Computer Vision and Pattern Recognition*, 6449–6458.

Wang, G.; Yuan, Y.; Chen, X.; Li, J.; and Zhou, X. 2018b. Learning discriminative features with multiple granularities for person re-identification. In *2018 ACM Multimedia Conference on Multimedia Conference*, 274–282. ACM.

Wang, X.; Girshick, R.; Gupta, A.; and He, K. 2018c. Non-local neural networks. In *Proceedings of the IEEE conference on computer vision and pattern recognition*, 7794–7803.

Wang, Y.; Wang, L.; You, Y.; Zou, X.; Chen, V.; Li, S.; Huang, G.; Hariharan, B.; and Weinberger, K. Q. 2018d. Resource aware person re-identification across multiple resolutions. In *Proceedings of the IEEE Conference on Computer Vision and Pattern Recognition*, 8042–8051.

Wei, L.; Zhang, S.; Gao, W.; and Tian, Q. 2018. Person transfer gan to bridge domain gap for person re-identification. In *Proceedings of the IEEE conference on computer vision and pattern recognition*, 79–88.

Zhang, G.; Zhang, P.; Jinqing, Q.; and Lu, h. 2021. HAT: Hierarchical Aggregation Transformers for Person Re-identification. In *2021 ACM Multimedia Conference on Multimedia Conference*. ACM.

Zhang, X.; Luo, H.; Fan, X.; Xiang, W.; Sun, Y.; Xiao, Q.; Jiang, W.; Zhang, C.; and Sun, J. 2018. Alignedreid: Surpassing human-level performance in person re-identification. *arXiv preprint arXiv:1711.08184v2*.

Zhang, Z.; Lan, C.; Zeng, W.; and Chen, Z. 2019. Densely Semantically Aligned Person Re-Identification. In *Proceedings of the IEEE Conference on Computer Vision and Pattern Recognition*, 667–676.

Zheng, L.; Huang, Y.; Lu, H.; and Yang, Y. 2019a. Pose invariant embedding for deep person re-identification. *IEEE Transactions on Image Processing*.

Zheng, L.; Shen, L.; Tian, L.; Wang, S.; Wang, J.; and Tian, Q. 2015. Scalable Person Re-identification: A Benchmark. In *Computer Vision, IEEE International Conference on Computer Vision*, 1116–1124.

Zheng, M.; Karanam, S.; Wu, Z.; and Radke, R. J. 2019b. Re-Identification with Consistent Attentive Siamese Networks. In *Proceedings of the IEEE Conference on Computer Vision and Pattern Recognition*, 5735–5744.

Zheng, Z.; Yang, X.; Yu, Z.; Zheng, L.; Yang, Y.; and Kautz, J. 2019c. Joint discriminative and generative learning for person re-identification. In *Proceedings of the IEEE/CVF Conference on Computer Vision and Pattern Recognition*, 2138–2147.

Zheng, Z.; Zheng, L.; and Yang, Y. 2017. Unlabeled samples generated by gan improve the person re-identification baseline in vitro. In *Proceedings of the IEEE International Conference on Computer Vision*, 3754–3762.

Zhong, Z.; Zheng, L.; Cao, D.; and Li, S. 2017a. Re-ranking person re-identification with k-reciprocal encoding. In *Proceedings of the IEEE Conference on Computer Vision and Pattern Recognition*, 1318–1327.

Zhong, Z.; Zheng, L.; Kang, G.; Li, S.; and Yang, Y. 2017b. Random erasing data augmentation. *arXiv preprint arXiv:1708.04896*.

Zhou, K.; Yang, Y.; Cavallaro, A.; and Xiang, T. 2019. Omni-scale feature learning for person re-identification. In *Proceedings of the IEEE/CVF International Conference on Computer Vision*, 3702–3712.

Zhu, K.; Guo, H.; Liu, Z.; Tang, M.; and Wang, J. 2020. Identity-Guided Human Semantic Parsing for Person Re-Identification. In *Proceedings of the European Conference on Computer Vision (ECCV)*, 346–363.